Excitation and propagation of torsional T(0,1) mode for guided wave testing of pipeline integrity

X. Niu[a,b], W. Duan[c], Hua-Peng Chen[b,*], H.R. Marques[d]

[a] *National Structural Integrity Research Centre, TWI Ltd, Cambridge CB21 6AL, UK.*
[b] *Department of Engineering Science, University of Greenwich, Chatham Kent ME4 4TB, UK.*
[c] *Department of Mechanical, Aerospace and Civil Engineering, Brunel University London, Uxbridge, Middlesex UB8 3PH, UK.*
[d] *Integrity Management Group, TWI Ltd. Granta Park, Cambridge CB21 6AL, UK.*
** Corresponding author. E-mail address: hp.chen@outlook.com*

Abstract

Guided wave testing is one of non-destructive testing techniques for pipeline inspection using low-frequency ultrasonic waves. Guided wave testing uses a set of equally placed piezoelectric transducers around a pipe, and the number of transducers in the array is a key factor for suppressing higher order flexural modes. This paper presents an effective approach for the excitation and propagation of torsional T(0,1) wave mode for detecting defects in a steel pipe by using finite element numerical simulations and experimental studies. From the numerical and experimental results, the optimised design for transducer arrangement is investigated. The relationship between defect type, dimension and transducer arrangement is also investigated. To validate the finite element modelling, the numerical results are then compared to the experimental data. Finally, the sensitivity of reflected signal from defects to two types of transducer array design is evaluated, and circumferential displacement along the pipe is investigated by using polar plots at different axial positions.

Keywords: Guided Wave; Piezoelectric Transducer Array; Finite Element Modelling; Wave Propagation; Pipeline Integrity.

1. Introduction

Pipelines have been widely used in industry and they need to be properly maintained for safe and reliable operation. Non-destructive testing (NDT) of pipelines using ultrasonic guided waves is particularly attractive because this technique could scan a relatively long section of pipe at a single access location. The commonly used NDT methods include X-ray inspection, ultrasonic testing (UT), guided wave (GW) testing and magnetic flux leakage (MFL) [1, 2]. For long range ultrasonic testing, guided waves work in a low operating frequency range from 20 kHz to 100 kHz [3]. Mudge and Speck [4] evaluated that a defect with a 3 - 9% area ratio of a pipe cross-section can be detected using GW testing. High level sensitivity of guided waves to defects is an area of interest for industry. In pipeline GW testing, generally a set of circumferential arrays, or "rings", is clamped around the pipe circumference. To suppress non-axisymmetric wave modes, the transducers are equally spaced around the cylindrical structure for the generation of a pure axisymmetric wave mode [5]. Then, the transmitted signal can form unidirectional propagation by using multiple rings [6, 7, 8].

Guided wave mode excitation and propagation for defect detection have been widely investigated. Gazis [9] investigated the propagation of fundamental and higher order flexural wave modes in pipes. Silk and Bainton [10] introduced a nomenclature of $\boldsymbol{X}(m,n)$ to describe these wave modes, in which $\boldsymbol{X}$ represents wave mode characteristics, namely L, T and F for longitudinal, torsional and flexural, respectively, m indicates the circumferential order, and n indicates the mode order of occurrence. The number of transducers used to generate different wave modes has been investigated in the literature. Volker and Vos [11] used 32 piezoelectric transducers for excitation of guided wave modes for pipe inspection. Rose [12] simulated a circumferential array composed of 8 transducers. Zhou et al. [13] modelled excitation with 1, 2, 8 and 32 piezoelectric transducers on the surface of an aluminium pipe to conduct the axisymmetric torsional wave generation and propagation. Miao et al. [14] presented the

circumferential displacement simulation of torsional wave mode T(0,1) by using 12 and 24 transducers. These results show that the number of transducers per ring has significant influence on the quality of the transmitted signal. To optimise the performance of transducer arrays without significant increase of costs, the transducer array design can be evaluated by finite element (FE) modelling [5, 15] and experimental studies [15, 16, 17].

This paper investigates the design of piezoelectric transducer arrays for guided wave testing. Finite element analyses are used to simulate different designs of piezoelectric transducer arrays. The excited signal from a one-ring transducer set-up is compared to that from a three-ring set-up. The experimental studies were carried out using a commercially available tool, consisting of three circumferential rings. Each ring is composed of 24 piezoelectric transducers, and the thickness-shear (d15) piezoelectric transducers are encapsulated in a collar. The collar has to be clamped and locked around the pipe, which leaves a gap of 33 degrees between the first and last transducer. However, the rest of the 22 transducers are evenly distributed. The sensitivity of received signal from defects to two transducer array designs is evaluated. Radial and axial displacements along the pipe are evaluated in numerical simulations and experimental studies, and circumferential displacement along the pipe is also investigated by using polar plots at different axial positions.

2. Theoretical background

2.1 Elastic wave propagation and excitation

The theoretical background is described in literature such as [12] for guided wave excitation and propagation in hollow cylinders. Typically, the pipe is assumed to have traction-free boundary condition, as shown in Fig. 1. The governing Navier's equation for guided wave propagation in an elastic medium is written here as

$$(\lambda+\mu)\nabla(\nabla\cdot\overline{U})+\mu\nabla^2\overline{U}=\rho\frac{\partial^2\overline{U}}{\partial t^2} \quad (1)$$

where λ and μ are Lamé constants, t is time and ρ is density, $\overline{U}$ is the displacement vector, ∇^2 is the three-dimensional Laplace operator.

Using a separation of variable technique, Ditri and Rose [18] expressed the displacement field as

$$v_r = R_r^{mn}(r)e^{im\theta}e^{i(\omega t-k^{mn}z)}\ ;\ v_\theta = R_\theta^{mn}(r)e^{im\theta}e^{i(\omega t-k^{mn}z)}\ ;\ v_z = R_z^{mn}(r)e^{im\theta}e^{i(\omega t-k^{mn}z)} \quad (2)$$

where the terms of v_r , v_θ and v_z are the components of displacement in the radial, circumferential and axial direction, respectively; $R_r^{mn}(r)$, $R_\theta^{mn}(r)$ and $R_z^{mn}(r)$ are the corresponding displacement amplitudes; The non-negative integer m (= 0, 1, 2, …) indicates the circumferential order, and n (=1, 2, 3, …) indicates the mode order of occurrence; ω is the radian frequency and $i = \sqrt{-1}$; and k^{mn} is the wave number in the axial direction.

Substitution of Eq. (2) into Eq. (1) leads to a characteristic equation, and solution of the characteristic equation delivers wavenumber solution of each mode. Equation (1) can also be solved numerically using a semi-analytical finite element (SAFE) technique. Figure 2 shows the results for phase and group velocity dispersion curves for an 8-inch schedule 40 steel pipe [19, 20, 21]. The outer diameter of the pipe is 219.1 mm, and wall thickness 8.18 mm. It can be seen that fundamental wave modes L(0,1), T(0,1) and L(0,2) are followed by three families of higher order modes F(m,1), F(m,2) and F(m,3), respectively. The torsional wave mode T(0,1) is widely excited for guided wave testing [3]. T(0,1) has a constant phase/group velocity, as shown in Fig. 2, therefore this wave is completely non-dispersive.

Modal amplitudes of excited wave modes are determined by the transducer arrangement. The amplitude of the wave mode $\boldsymbol{X}(m,n)$ in the positive propagation direction is obtained by applying the loading conditions. The positive amplitude can be expressed here as [18, 22]:

$$A_{+}^{mn} = -\frac{R_{\xi}^{mn}(r)e^{-ik^{mn}z}r_{n+1}}{4P_{mmnn}}\int_{-\alpha}^{-\alpha+2\pi} e^{im\theta}p_1(\theta)d\theta\int_{-\infty}^{\infty} p_2(z)e^{ik^{mn}z}dz \tag{3}$$

where $R_{\xi}^{mn}(r)$ (ξ = 1, 2, 3) represents amplitude in the dominant vibration direction; and P_{mmnn} represents the orthogonality relation between two modes. As shown in Fig. 1, r_1 and r_2 represent inner radius and outer radius, respectively. The loading area is 2α (circumferential length) × $2L$ (axial length), and $p_1(\theta)$ and $p_2(z)$ represent circumferential and axial loading distribution functions, respectively. The angular profiles can be obtained by summing up the angular profile of each mode in a family with weighting functions A_{+}^{mn}, which are the amplitudes calculated from Eq. (3). In a finite element procedure, the governing equations can be decomposed differently. The detailed numerical procedure is described in [23] and [24].

2.2 *Numerical T(0,1) excitation and wave superposition*

In the FE model, a Hanning-windowed tone burst T(0,1) signal is generated, and the time domain incident signal is expressed as

$$u(t) = \frac{1}{2}[1-\cos(\frac{2\pi f_c t}{n_c})]\sin(2\pi f_c t) \tag{4}$$

where t is time, f_c is the centre frequency of the incident signal, and n_c is the number of signal cycles. From harmonic analysis using ABAQUS, mode shapes of T(0,1) and F(1,2) are obtained and shown in Fig. 3.

A 10-cycle Hanning-windowed sinusoidal signal at 35 kHz is excited by using piezoelectric transducer arrays. Furthermore, T(0,1) is generated in a single direction. The backward propagating T(0,1) wave mode is suppressed by using multiple transducer arrays. In general, two or three rings can be used to form a unidirectional T(0,1) wave mode. In this paper, the ring spacing of 30 mm is adopted between multiple rings. For the arrangement of two transducer rings, the first ring (Ring 1) is excited by a pulse signal, and the excitation signal of the second ring (Ring 2) is inverted when compared to the signal of Ring 1. The signal of Ring

2 is also time-delayed, and the delay time is the value of ring spacing 30 mm divided by group velocity of wave mode T(0,1). For the arrangement of three rings of transducers, the time domain signal of Ring 1 is given by Eq. (4). A 35 kHz, 10-cycle Hanning windowed pulse is employed here, as shown in Figs. 4(a) and 4(b). These displacements are normalised with respect to the amplitude of the incident signal, thus they are dimensionless quantities. The signal of Ring 2 is inverted, and its signal amplitude is twice of Ring 1. The signal is also time-delayed with a value of 30 mm divided by group velocity of wave mode T(0,1), i.e. 3260 m/s for this case. The signal of Ring 3 is the same as the signal of Ring 1, and it is also time-delayed with a value of twice the ring spacing, i.e. 60 mm, divided by 3260 m/s.

2.3 Modelling of absorbing regions using increased mass-proportional damping

To model the absorbing regions for the boundaries of guided waves in pipes, the finite element simulations can be carried out by using gradually increasing damping. For the Rayleigh damping composed of mass-proportional damping and stiffness-proportional damping, the damping matrix can be expressed as

$$[C] = \alpha [M] + \beta [K] \tag{5}$$

where [M] and [K] are the mass and stiffness matrices, respectively; α and β are mass-proportional and stiffness-proportional damping, respectively. The related effect of the Rayleigh coefficients α and β on the effective damping ratio ξ can be illustrated with a simplified single degree of freedom system, given here as

$$\xi = \frac{1}{2}\left(\frac{\alpha}{\omega} + \beta\omega\right) \tag{6}$$

where ω represents the natural frequency at a given mode. It is obvious that α is more effective at damping low frequency signals, while β is more effective at damping high frequency signals [25, 26]. In this paper, damping layers with gradually increasing coefficient α are used to build the absorbing regions [27, 28, 29, 30], as shown in Fig. 5. Thus, the value of α_n at the *n*th

damping layer can be estimated from

$$\alpha_n = \omega\left(\frac{l_n}{L_{total}}\right)^3,\ n = 1,2,3,...,N \tag{7}$$

where $\omega = 2\pi f$; l_n is the distance from the starting boundary of the absorbing region to the centre of *n*th damping layer, as shown in Fig. 5; L_{total} represents the total length of the absorbing region; and *N* is the total number of damping layers. The direction of the increased values of the mass-proportional damping is the same as the wave propagation direction.

The total length of the absorbing region (L_{total} = 600 mm) is at least six times of the wavelength of the pulse signal at 35 kHz. The length of each individual layer is taken as 4 mm, close to the mesh size of the FE model in the axial direction. By using a longer length of the absorbing region, the method can be used to suppress a linear chirp signal that sweeps linearly from low to high frequency (or vice-versa).

3. Finite element modelling

The finite element modelling for the guided wave propagation along a 5 m long, 8-inch schedule 40 steel pipe is illustrated by using finite element software ABAQUS Explicit, as shown in Fig. 6. The pipe is modelled as a linear isotropic material with a mass density ρ = 7932 kg/m^3, Young's modulus E = 216.9 GPa and Poisson's ratio v = 0.2865. Three rings of transducers are placed at the left part of the pipe, and Ring 3 is located at 625 mm away from the left pipe end. Two different types of loading sources are used, i.e., point and line sources. For the point source set-up, each ring includes 24 evenly distributed point sources. For the line source set-up, each ring includes a line source enclosing the pipe circumference. The line source has a width of 4 mm. The point or line sources provide surface shear force loading in the circumferential direction. The ring spacing for two adjacent rings is 30 mm for both point and line sources. The transmitted signal is recorded using 24 points around the circumferential

of the pipe, located at 300 mm, 1300 mm and 2300 mm away from a simulated defect, respectively. To ensure a minimum of eight elements per wavelength in the axial direction for satisfactory accuracy [31], 881,276 hexahedron elements are generated for the point source set-up, and 882,684 elements are generated for the line source set-up. An average mesh size of 4 mm is used in the axial direction and four elements are used in the pipe wall thickness direction. The step time is 100 ns and the total calculation time is 2.3 ms.

Figure 7 shows the results for torsional T(0,1) waves generated by point and line sources, respectively. Three rings of sources are used in the numerical simulations, thus the waves only propagate in the forward direction. From the results, a pure torsional mode T(0,1) is generated by using the arrangement of the three rings of transducers in the numerical simulations. The amplitude of the signal excited by line source is greater than that of the signal excited by point source, as expected. In Fig. 8, three notches with various dimensions are simulated. Fig. 8(a) shows an outer notch with a depth of 50% of the pipe wall thickness. Fig. 8(b) is a through-thickness notch, and Fig. 8(c) is an inner notch with a 50% depth. The length for all these three notches is 12 mm in the axial direction, and the width is 86.1 mm in the circumferential direction. These notches are assumed to be at the top of the pipe.

Figure 9 shows the torsional T(0,1) wave mode propagating along the pipe and scattered due to various notches. Higher order flexural wave modes are generated and superimposed with the T(0,1) wave mode. The results show that the through-thickness notch produces the highest reflected signal. The reflected signal from the outer notch is slightly larger than that from the inner notch.

Figure 10 shows the results for the normalised circumferential, radial and axial displacements over time for No.1 receiver at the position shown in Fig. 6. The receiver is measured at 1300 mm away from the through-thickness notch, and it is placed at 82.5 degrees in the pipe profile. The duration of transmitted signal is 286 μs, and the travelling time is 2.25

ms. Results show that only T(0,1) wave mode is generated and then reflected from the through-thickness notch in the circumferential direction.

Figure 11 shows the incident and reflected T(0,1) wave from three notches in the pipe, where the simulation time is 2.25 ms. The time domain signal is obtained by summing and averaging signals recorded at 24 positions around the circumference of the pipe. The reflection coefficients are 7.9% for the outer notch, 16.1% for the through-thickness notch and 6.8% for the inner notch, respectively. Figure 12 shows angular profiles of the torsional T(0,1) mode superimposed with flexural modes for the reflected signal from three different notches. The normalised circumferential displacements are located at z = 0.3 m, 1.3 m and 2.3 m, respectively. It can be seen that the angular profile changes significantly when the notch changes. The amplitude of the through-thickness notch is much larger than that of the other two notches.

4. Experimental validation

To verify the modelling result, a test rig was designed (illustrated in Fig. 13) and experiments were carried out for the pipe shown in Fig. 14 [16]. The torsional wave mode T(0,1) was excited by three rings of thickness-shear (d15) piezoelectric transducers. A 4450 mm long, 8-inch schedule 40 steel pipe was used for the experimental study. The piezoelectric transducers were driven by a Teletest® MK3 system. The signal was recorded by a CLV-3D laser vibrometer system located at 2000 mm away from the pipe end. The laser vibrometer measured circumferential displacements at 24 points evenly distributed around the pipe circumference from 20 kHz to 60 kHz.

Figure 15 shows the comparison of the normalised circumferential, radial and axial displacements by averaging results from 24 receiving points, which are obtained from experiments and simulations for the transmitted signal at 35 kHz. There is excellent agreement

between experimental and simulated results. The fundamental wave mode T(0,1) was generated in the circumferential direction. Note that there is a 33-degree gap between the first and last transducers in each ring, as shown in Fig. 13, and the remaining transducers are evenly distributed. Due to this gap, higher order modes may be generated, and the circumferential displacements are not exactly axisymmetric.

Figure 16 shows the comparison of the normalised circumferential displacements in polar plots obtained from experimental measurements and FE modelling. The FE modelling for the guided wave excitation and propagation for pipe inspection is then examined using the experimental data. From the results, there is a good agreement between the experimental results and the FE simulations. For the selection of frequency range, 35 kHz is an appropriate testing frequency due to the effects of non-uniform distribution of transducers in each ring and 30 mm ring spacing for this experimental set-up. Also, the circumferential displacements are non-uniform at 24 receivers, as shown in the polar plots, since there is a gap between start and end transducers of the array. The flexural F(1,2) has a higher contribution than other flexural wave modes for the non-axisymmetric transducer arrays.

5. Conclusions

In this paper, two transducer ring set-ups, i.e., point and line sources are investigated for pipeline guided wave testing. Finite element method is used to model the difference of these two source set-ups. An absorbing region method is used to suppress waves reflected from the pipe end, and a three-ring system is used to generate a T(0,1) mode that travels in one direction only. Three different notches are introduced into the pipe, and the reflected signals from these notches are examined in time domain signals and polar plots. The appearance of high order modes is clear. The numerical results are validated experimentally. It can be seen that non-uniform distribution of transducers around the pipe will generate higher order non-

axisymmetric modes.

Acknowledgments

This publication was made possible by the sponsorship and support of TWI Ltd. and University of Greenwich. The work was enabled through, and undertaken at, the National Structural Integrity Research Centre (NSIRC), a postgraduate engineering facility for industry-led research into structural integrity established and managed by TWI through a network of both national and international Universities.

References

[1] V. Suresh, A. Abudhahir, D. Jackson, Development of magnetic flux leakage measuring system for detection of defect in small diameter steam generator, Measurement 95 (2017) 273-279.

[2] H.-P. Chen, Structural Health Monitoring of Large Civil Engineering Structures, John Wiley & Sons Limited, Oxford, UK, 2018.

[3] P. Mudge, Field application of the Teletest long-range ultrasonic testing technique, Insight - Non-Destructive Testing and Condition Monitoring 43 (2001) 74-77.

[4] P. Mudge, J. Speck, Long-range ultrasonic testing (LRUT) of pipelines and piping, Inspectioneering Journal 10 (2004) 1.

[5] X. Niu, H.-P. Chen, H.R. Marques, Piezoelectric transducer array optimization through simulation techniques for guided wave testing of cylindrical structures, in The 8th ECCOMAS Thematic Conference on Smart Structures and Materials (SMART 2017), Madrid, Spain, 2017.

[6] D. Alleyne, P. Cawley, Long range propagation of Lamb waves in chemical plant pipework, Materials Evaluation 55 (1997) 504-508.

[7] P. Cawley, Practical guided wave inspection and applications to structural health monitoring, in Proceedings of the 5th Australasian Congress on Applied Mechanics (ACAM 2007), 2007.

[8] X. Niu, H.R. Marques, H.-P. Chen, Sensitivity analysis of circumferential transducer array with T(0,1) mode of pipes, Smart Structures and Systems 21 (2018) 761-776.

[9] D.C. Gazis, Three dimensional investigation of the propagation of waves in hollow circular cylinder. I. Analytical foundation, The Journal of the Acoustical Society of America 31 (1959) 568-573.

[10] M. Silk, K. Bainton, The propagation in metal tubing of ultrasonic wave modes equivalent to lamb waves, Ultrasonics 17 (1979) 11-19.

[11] A. Volker, H. Vos, Experimental results of guided wave travel time tomography, in AIP Conference Proceedings, 2012.

[12] J.L. Rose, Ultrasonic Guided Waves in Solid Media, Cambridge University Press, Cambridge, 2014.

[13] W. Zhou, F.-G. Yuan, T. Shi, Guided torsional wave generation of a linear in-plane shear piezoelectric array in metallic pipes, Ultrasonics 65 (2016) 69-77.

[14] H. Miao, Q. Huan, Q. Wang, F. Li, Excitation and reception of single torsional wave T(0,1) mode in pipes using face-shear d24 piezoelectric ring array, Smart Materials and Structures 26 (2017) 9.

[15] S. Lowe, S. Fateri, R. Sanderson, N.V. Boulgouris, Finite element modelling of the interaction of ultrasonic guided waves with coupled piezoelectric transducers, Insight - Non-Destructive Testing and Condition Monitoring 56 (2014) 505-509.

[16] X. Niu, H.R. Marques, H.-P. Chen, Transducer array optimisation for guided wave testing of pipes using finite element numerical simulations and experimental studies, in The 8th International Conference on Structural Health Monitoring of Intelligent Infrastructure (SHMII8), 2017.

[17] P.S. Lowe, R.M. Sanderson, N.V. Boulgouris, A.G. Haig, W. Balachandran, Inspection of cylindrical structures using the first longitudinal guided wave mode in isolation for higher flaw sensitivity, IEEE Sensors Journal 16 (2016) 706-714.

[18] J. Ditri, J.L. Rose, Excitation of guided elastic wave modes in hollow cylinders by applied surface tractions, Journal of Applied Physics 72 (1992) 2589-2597.

[19] W. Duan, R. Kirby, A numerical model for the scattering of elastic waves from a non-axisymmetric defect in a pipe, Finite Elements in Analysis and Design 100 (2015) 28-40.

[20] W. Duan, R. Kirby, P. Mudge, On the scattering of elastic waves from a non-axisymmetric defect in a coated pipe, Ultrasonic 65 (2016) 228-241.

[21] W. Duan, R. Kirby, P. Mudge, On the scattering of torsional waves from axisymmetric defects in buried pipelines, The Journal of the Acoustical Society of America 141 (2017) 3250-3261.

[22] J. Li, J.L. Rose, Excitation and propagation of non-axisymmetric guided waves in a hollow cylinder, The Journal of the Acoustical Society of America 109 (2001) 457-464.

[23] J. Hua, J. Mu, J.L. Rose, Guided wave propagation in single and double layer hollow cylinders embedded in infinite media, The Journal of the Acoustical Society of America 129 (2011) 691-700.

[24] W. Duan, R. Kirby, P. Mudge, T.-H. Gan, A one dimensional numerical approach for computing the eigenmodes of elastic waves in buried pipelines, Journal of Sound and Vibration 384 (2016) 177-193.

[25] C.-H. Liu, K.-M. Lee, Dynamic modeling of damping effects in highly damped compliant fingers for applications involving contacts, Journal of Dynamic Systems, Measurement, and Control 134 (2011) 011005-9.

[26] X. Chen, J. Duan, H. Qi , Y. Li, Rayleigh damping in Abaqus/Explict dynamic analysis, Applied Mechanics and Materials 627 (2014) 288-294.

[27] M. Castaings, C. Bacon, Finite element modeling of torsional wave modes along pipes with absorbing materials, The Journal of the Acoustical Society of America 119 (2006) 3741-3751.

[28] M. Castaings, M. Lowe, Finite element model for waves guided along solid systems of arbitrary section, The Journal of the Acoustical Society of America 123 (2008) 696-708.

[29] A. Velichko, P.D. Wilcox, A generalized approach for efficient finite element modeling of elastodynamic scattering in two and three dimensions, The Journal of the Acoustical Society of America 128 (2010) 1004-1014.

[30] J.R. Pettit, A. Walker, M.J.S. Lowe, An optimised stiffness reduction method for simulating infinite elastic space using commercial finite elements codes, Journal of Physics: Conference Series 581 (2015) 012005.

[31] D.N. Alleyne, M.J.S. Lowe, P. Cawley, The reflection of guided waves from circumferential notches in pipes, Journal of Applied Mechanics, 65 (1998) 635-641.

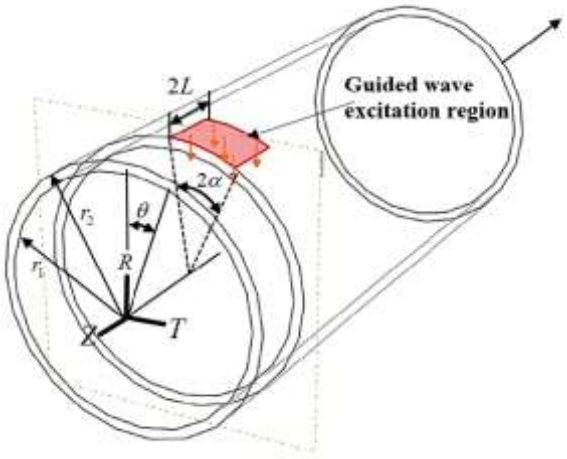

Figure 1. A piezoelectric transducer placed on top of an elastic pipe.

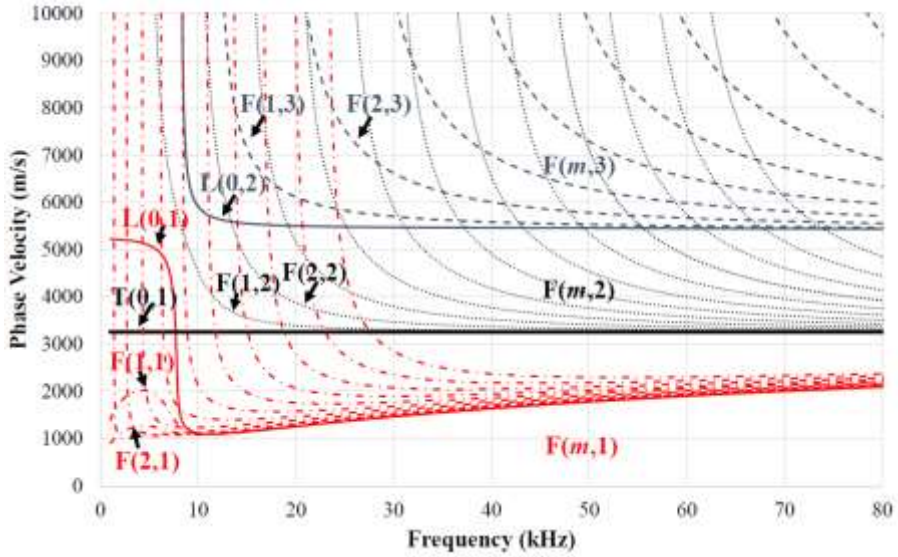

(a) phase velocity

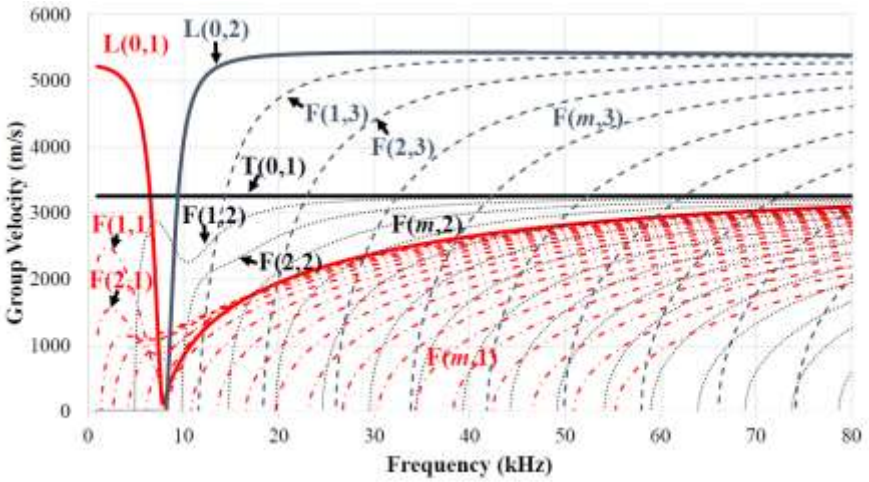

(b) group velocity

Figure 2. Dispersion curves for an 8-inch schedule 40 steel pipe.

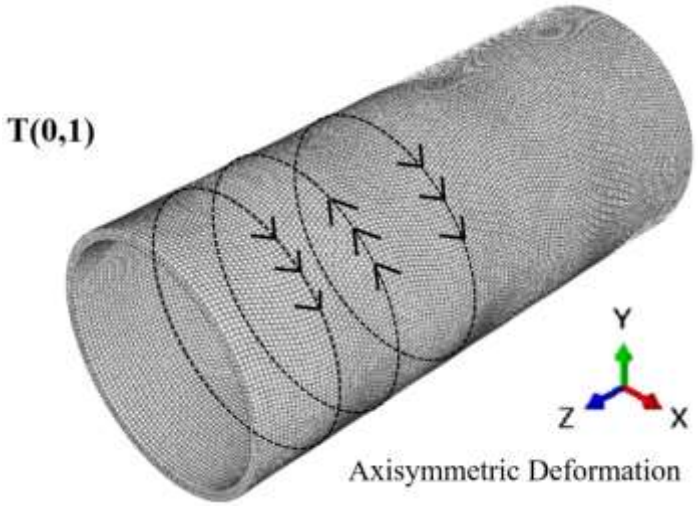

(a) Longitudinal wave mode T(0,1)

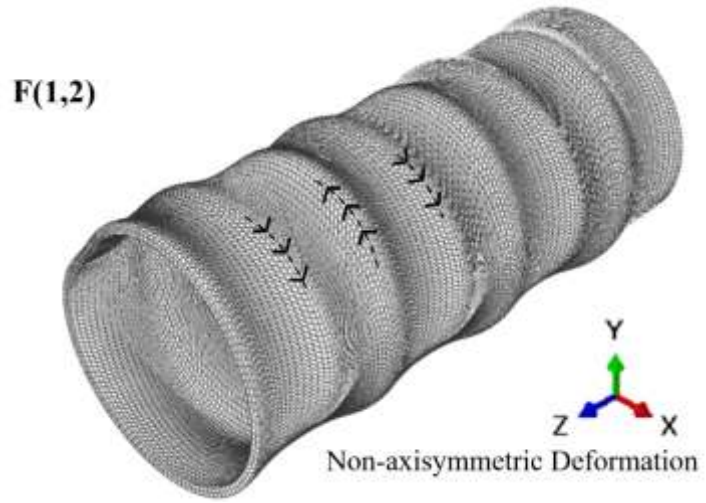

(b) Flexural wave mode F(1,2)

Figure 3. Mode shapes in an 8-inch schedule 40 pipe.

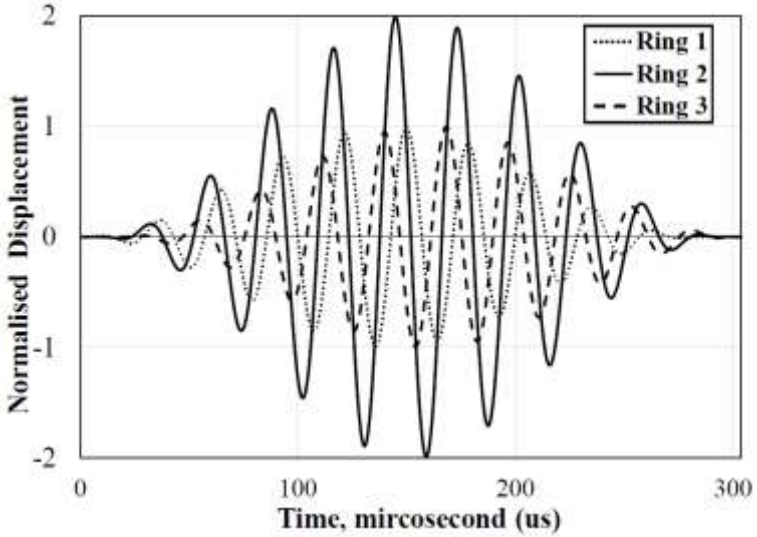

(a) Time domain

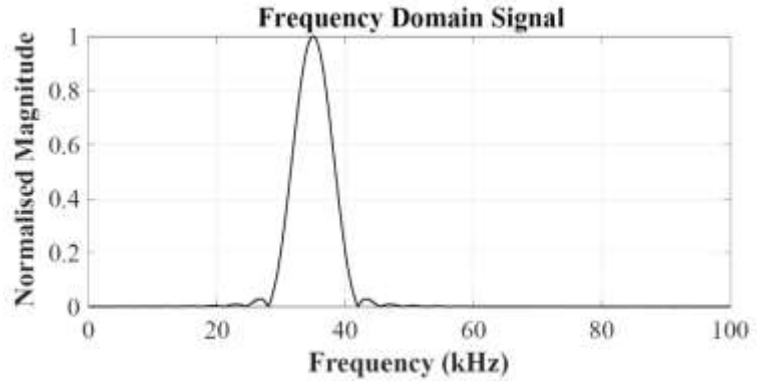

(b) Frequency spectrum

Figure 4. Incident signal used for three transducer rings.

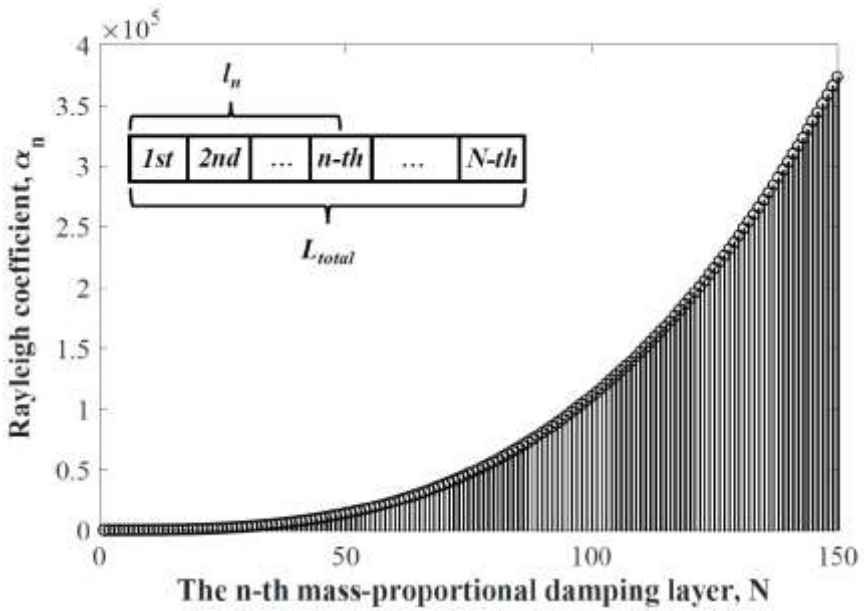

Figure 5. The mass-proportional damping coefficients related to damping layers.

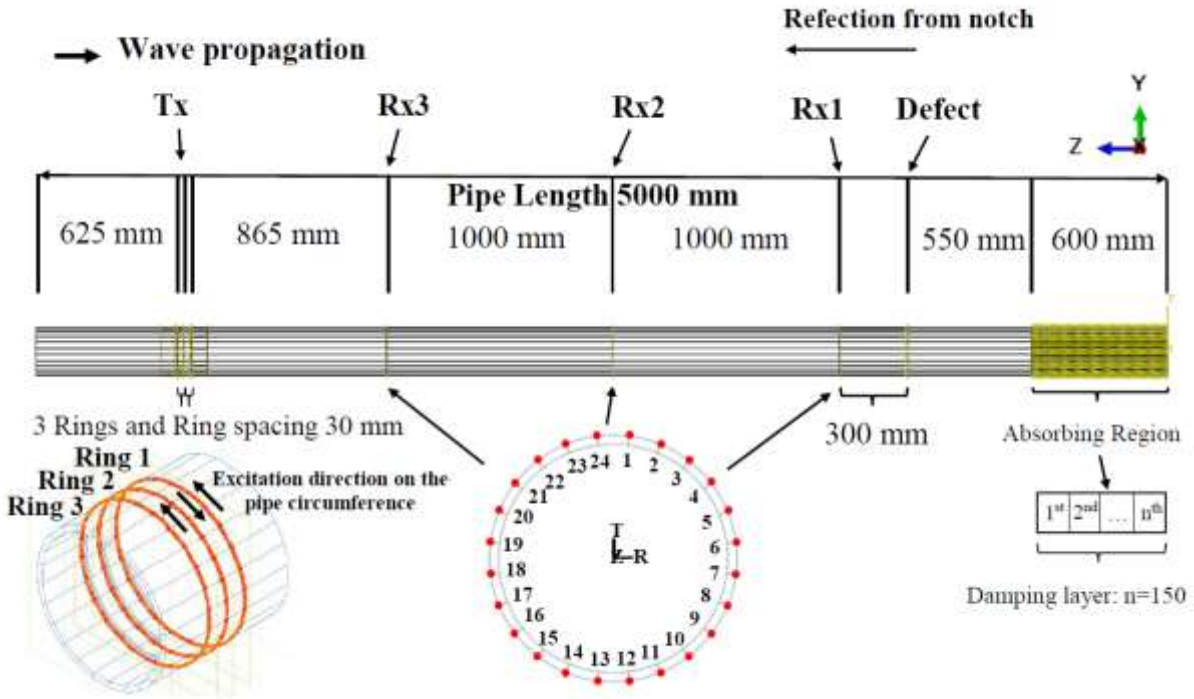

Figure 6. Finite element modelling for an 8-inch, schedule 40 steel pipe with two different types of transducer arrays.

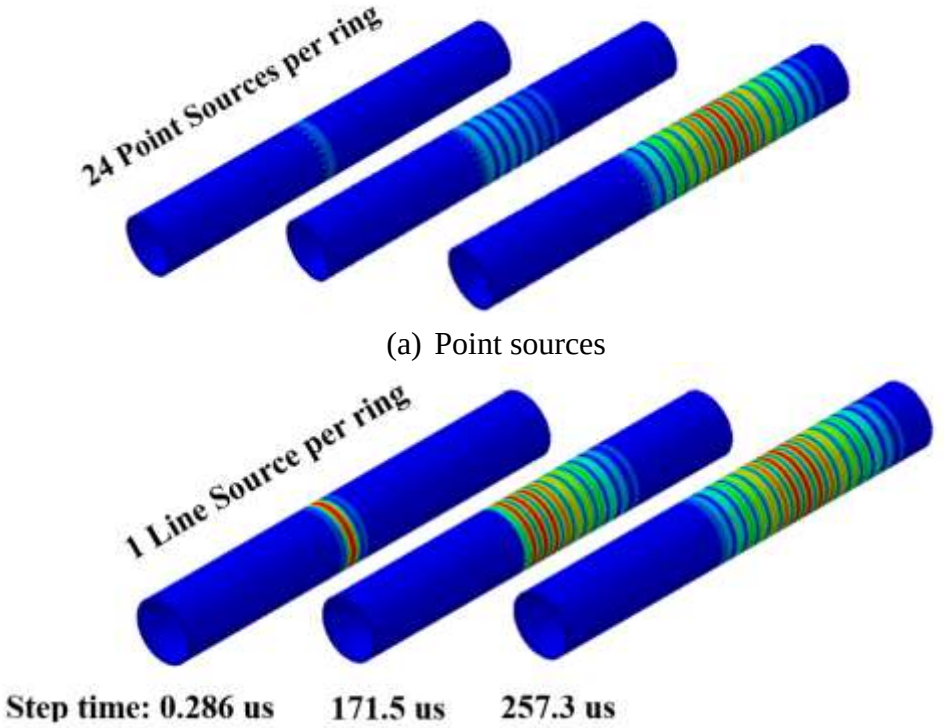

(a) Point sources

(b) Line sources

Figure 7. Excitation of torsional T(0,1) mode by two different transducer set-ups.

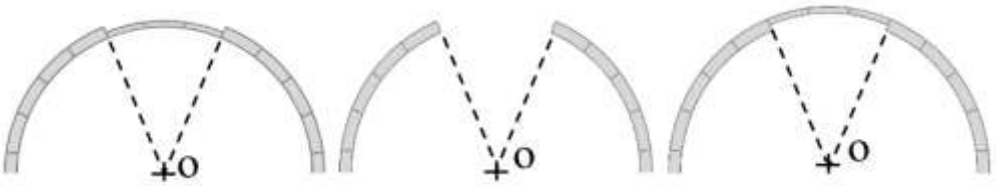

(a) (b) (c)

Figure 8. Three notches used in FE modelling: (a) Outer notch, (b) through-thickness notch, (c) inner notch.

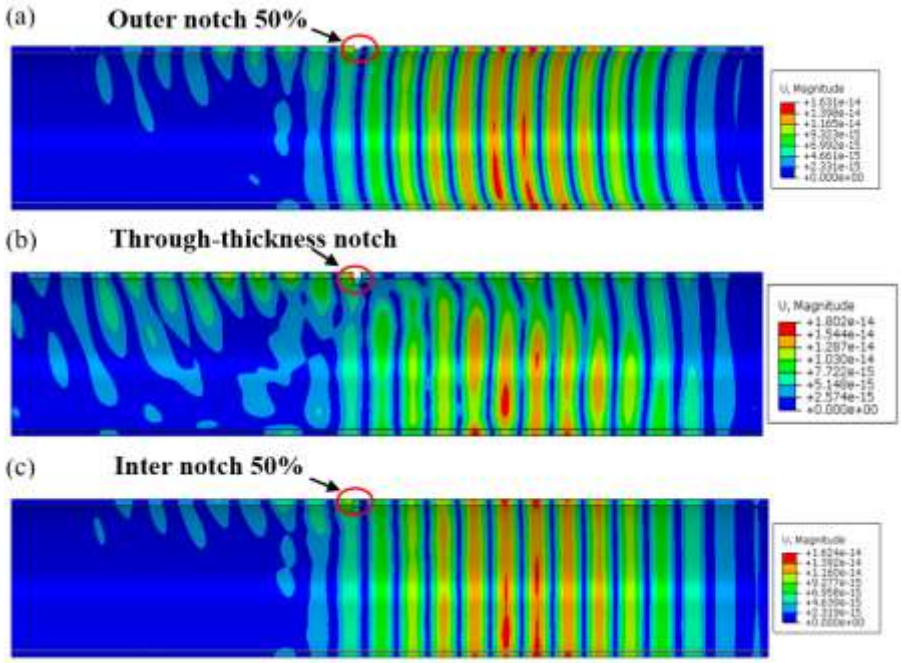

Figure 9. Scattering of T(0,1) by three different notches: (a) outer notch, (b) through-thickness notch, (c) inner notch.

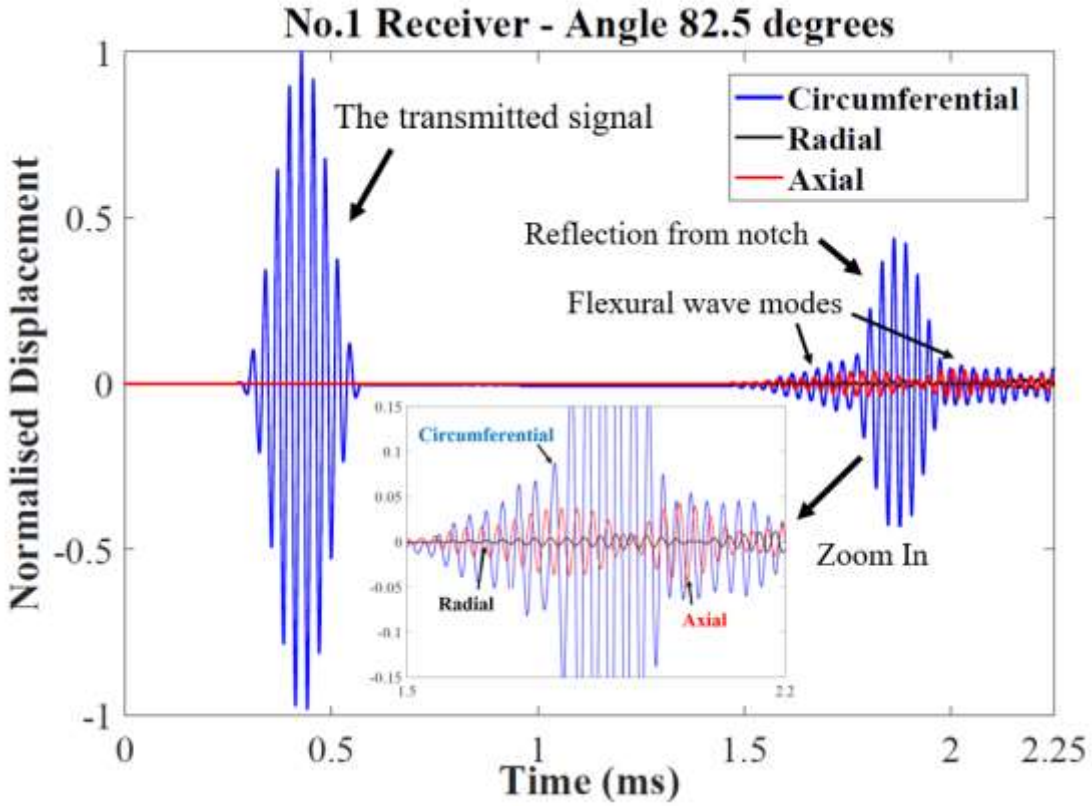

Figure 10. Time domain incident and reflected wave modes for through-thickness notch at No.1 receiver.

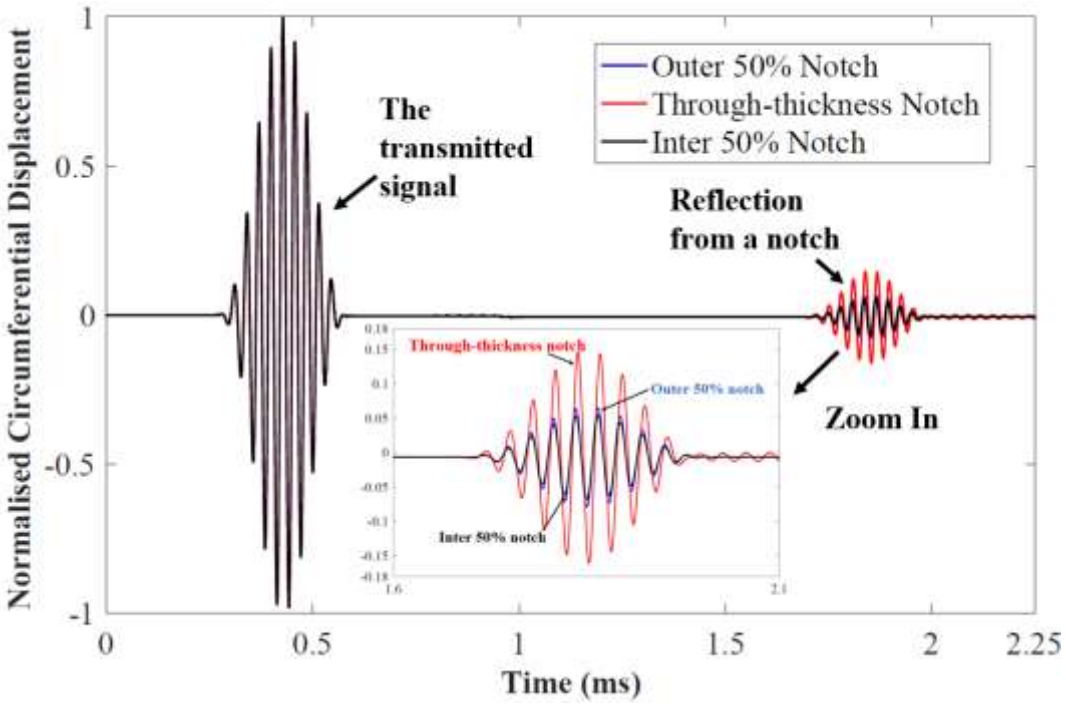

Figure 11. Time domain incident and reflected T(0,1) for three notches.

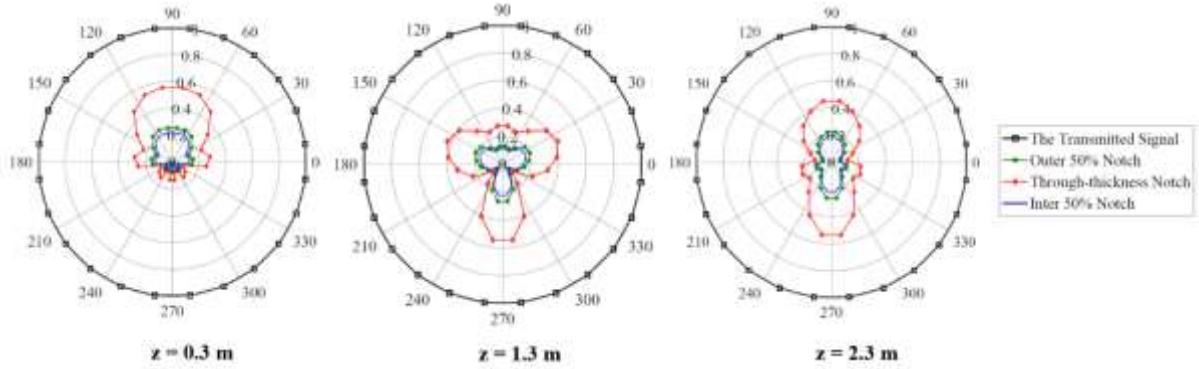

Figure 12. Angular profile of normalised circumferential displacement for the reflected signal from various notches at different locations.

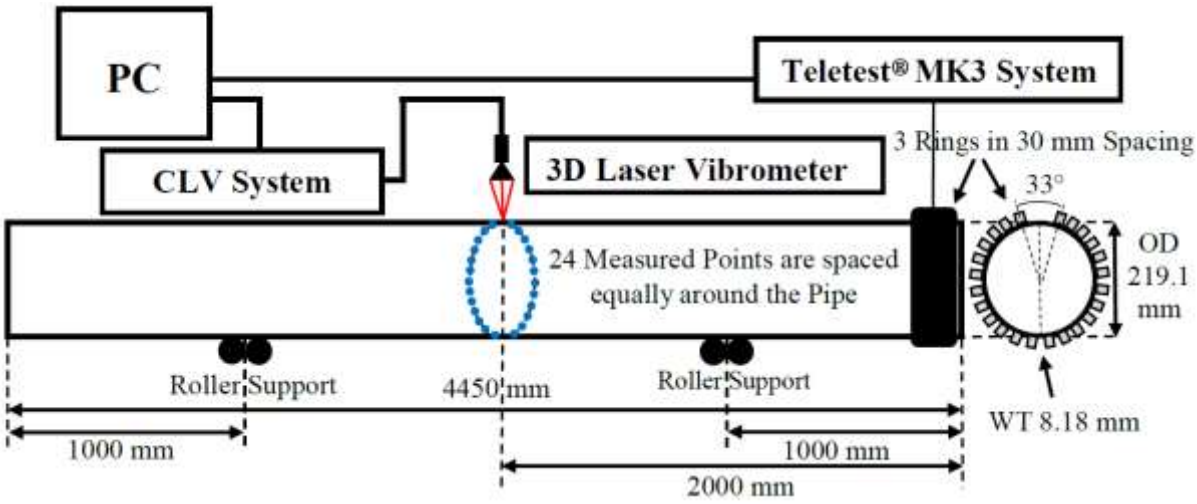

Figure 13. Schematic diagram of experimental set-up.

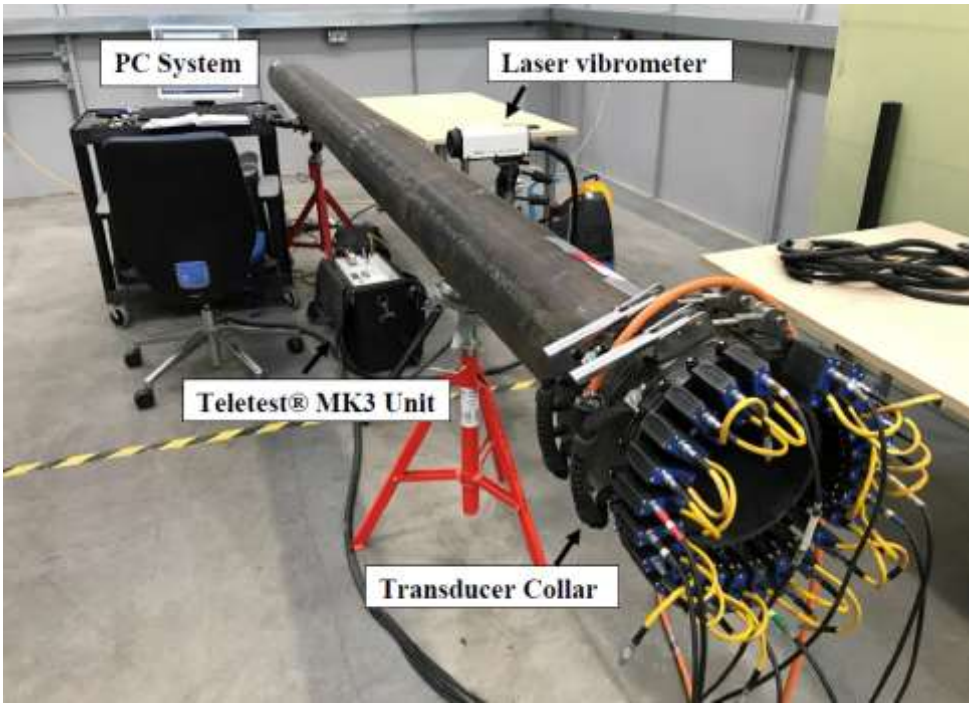

Figure 14. Test rig for generation and measurement of T(0,1).

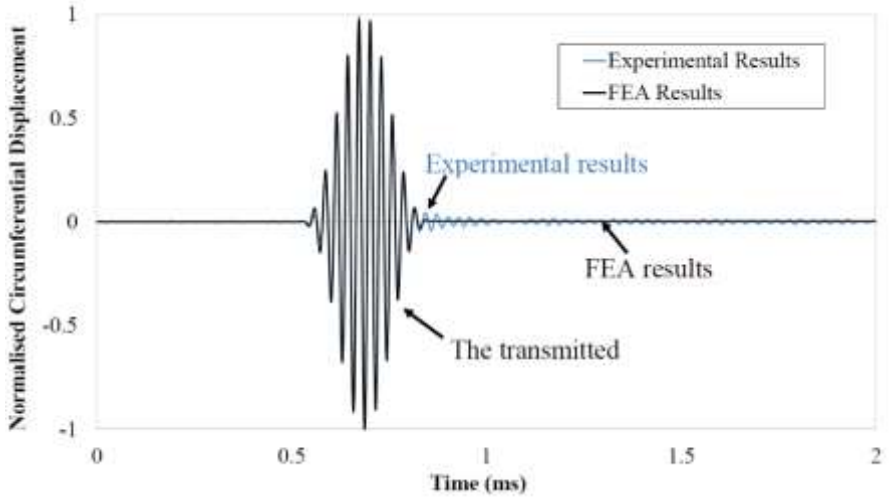

(a) Circumferential direction

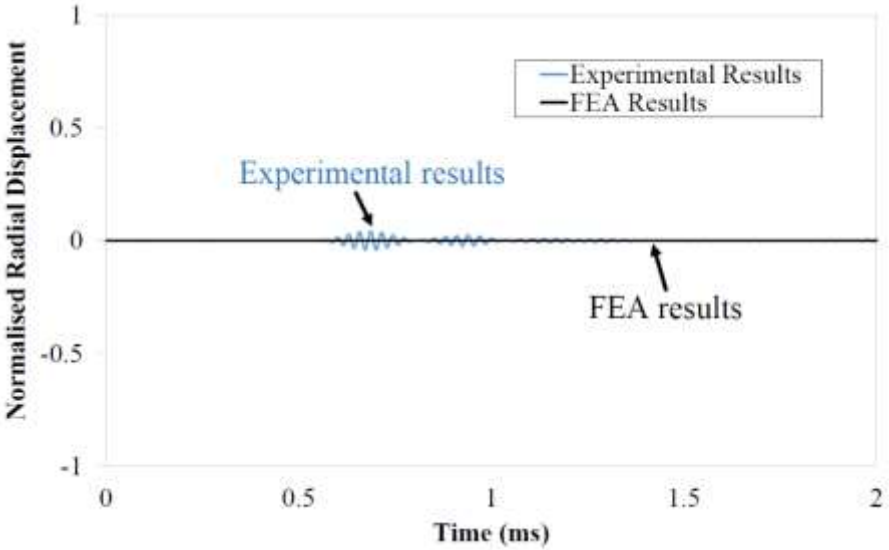

(b) Radial direction

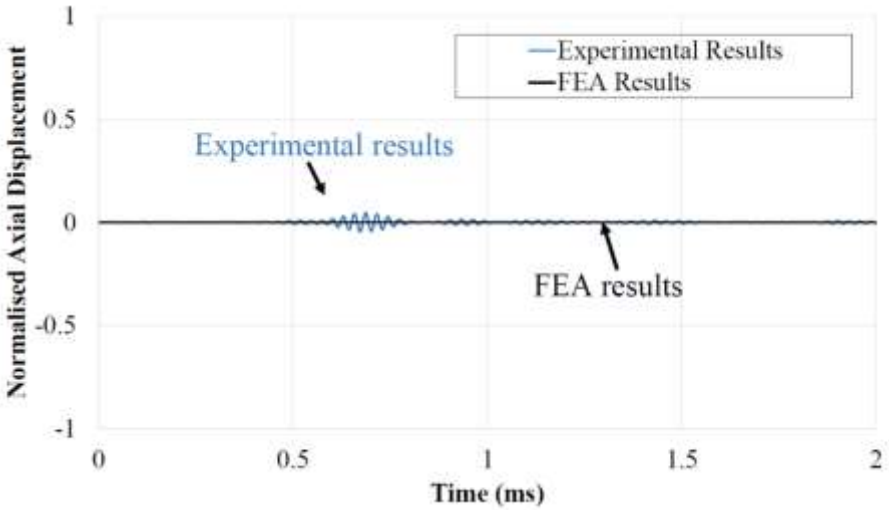

(c) Axial direction

Figure 15. Normalised circumferential, radial and axial displacements obtained from experimental data and numerical simulations.

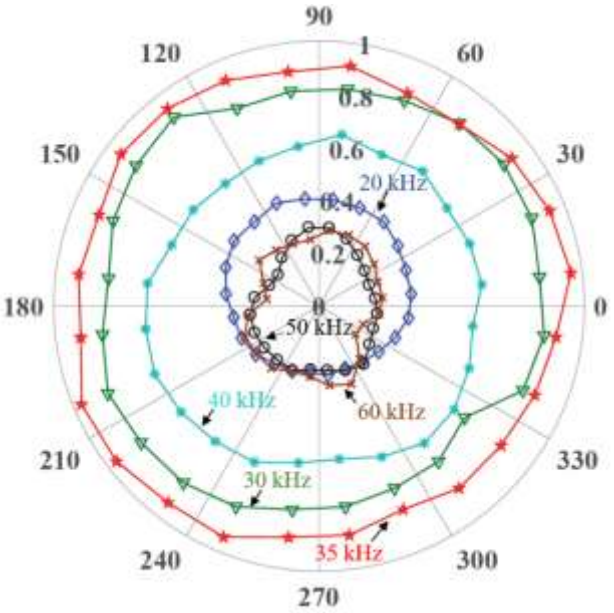

(a) Experimental results

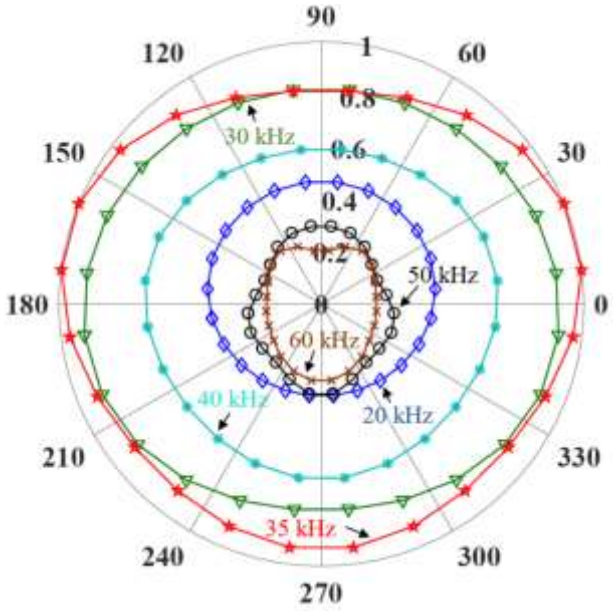

(b) Numerical predictions

Figure 16. Normalized circumferential displacements form experimental and numerical results.